nature neuroscience

SUPPLEMENTARY INFORMATION

https://doi.org/10.1038/s41593-019-0354-y

In the format provided by the authors and unedited.

A whole-brain atlas of monosynaptic input targeting four different cell types in the medial prefrontal cortex of the mouse

Sofie Ährlund-Richter[1,4], Yang Xuan[1,4], Josina Anna van Lunteren[2], Hoseok Kim[1], Cantin Ortiz[1], Iskra Pollak Dorocic[1,3], Konstantinos Meletis[1] and Marie Carlén[1,2*]

[1]Department of Neuroscience, Karolinska Institutet, Stockholm, Sweden. [2]Department of Biosciences and Nutrition, Karolinska Institutet, Huddinge, Sweden. [3]Present address: Department of Molecular and Cell Biology, University of California, Berkeley, Berkeley, CA, USA. [4]These authors contributed equally: Sofie Ährlund-Richter, Yang Xuan. *e-mail: marie.carlen@ki.se

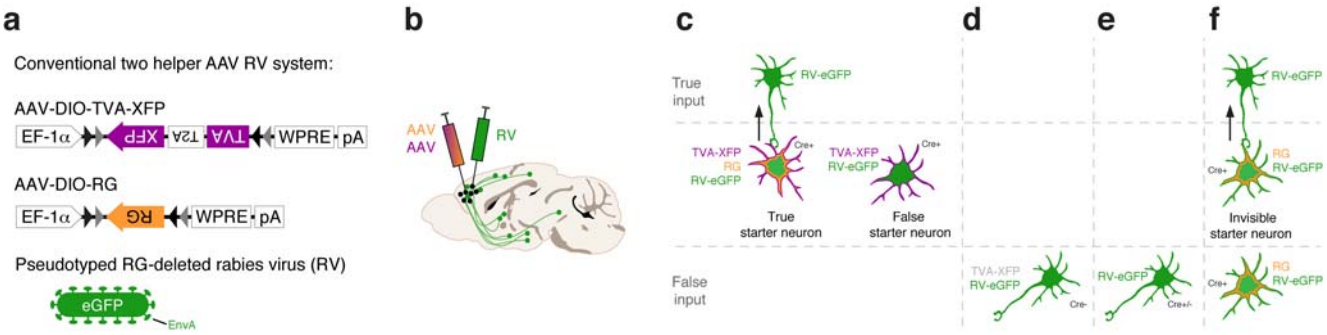

Supplementary Fig. 1

Outline of possible caveats and limitations in retrograde trans-synaptic RV tracing using two helper AAVs

(**a**) Efficient production and detection of starter neurons, i.e., the neurons whose presynaptic inputs are to be traced, are pivotal to successful RV tracing of circuitry, as is specific labeling of true input neurons, i.e., presynaptic neurons giving direct input to the starter neurons. The most commonly used RV systems employ RG-deleted RV particles pseudotyped to express the envelope protein EnvA. Viruses expressing EnvA use the TVA receptor for entry into cells, and selective expression of the TVA receptor in the starter neurons ensures that the initial RV transduction exclusively targets the neurons whose monosynaptic inputs are being traced. Production, and transsynaptic retrograde spread of RV particles to presynaptic neurons are dependent on *trans*-complementation of RG in the starter neurons. Regularly, two helper AAV vectors are used for cell-type-specific Cre-dependent expression of TVA and RG – most often one AAV vector expresses the TVA receptor and a fluorescent marker (TVA-XFP) in a Cre-dependent manner, while the second AAV, with Cre-dependent expression of RG, lacks a detectable marker[1-6]. This strategy precludes confirmation of RG expression in the starter neurons.
(**b**) The two AAVs are mixed and injected together, which does not guarantee co-expression of TVA and RG in all starter neurons[7].
(**c-f**) Illustration of possible misidentification of starter and/or input neurons in RV tracing using two AAVs with Cre dependent expression of TVA-XFP (1st AAV), and RG (2nd AAV). In the examples the RV expresses eGFP (RV-eGFP).
(**c**) True starter neurons express TVA and RG, are transduced by RV-eGFP, and can give rise to retrograde trans-synaptic RV-eGFP spread to presynaptic partners. False starter neurons cannot give rise to RV-eGFP labeled input. Neurons expressing TVA and RV-eGFP, but not RG, are an example of false starter neurons. Identification of starter neurons based of co-expression of the fluorophore in the TVA-XFP and the fluorophore encoded by the RV would include both true and false starter neurons, potentially resulting in an overestimation of the starter population and skewing of calculations of input neuron-starter neuron ratios. Further, reliable detection of (true) starter neurons is necessary for tracing of monosynaptic input in the local circuit[8,9].
(**d**) Expression of TVA in the absence of Cre has been reported, and low levels of TVA are sufficient for binding and integration of RV[1,9,10]. Importantly, the cell type specificity of the starter neurons can then be lost. As the low expression of the fluorophore in the TVA-construct cannot be detected[1], the RV transduced neurons can only be detected by the fluorophore expressed from the RV, identifying them as input neurons rather than starter neurons (i.e., they are false input neurons).
(**e**) Impure RV batches can result in TVA-independent RV transduction of neurons at the injection site. The transduced neurons are falsely identified as local input neurons based on the expression of the fluorophore in the RV.
(**f**) If a neuron expressing RG, but not TVA-XFP, is transduced by RV in an TVA-independent manner, it can give rise to RV labeling of its input neurons, and thus function as an invisible starter neuron. As the RG-expression is dependent on Cre recombination, trans-synaptically labeled input neurons would represent true input neurons. However, the invisible starter neuron (expressing RG) would be falsely identified as an input neuron, as only the fluorophore in the RV is expressed in this neuron.

References

1 Zhang, S. *et al.* Organization of long-range inputs and outputs of frontal cortex for top-down control. *Nature neuroscience* **19**, 1733-1742, doi:10.1038/nn.4417 (2016).
2 Pollak Dorocic, I. *et al.* A whole-brain atlas of inputs to serotonergic neurons of the dorsal and median raphe nuclei. *Neuron* **83**, 663-678, doi:10.1016/j.neuron.2014.07.002 (2014).
3 Watabe-Uchida, M., Zhu, L., Ogawa, S. K., Vamanrao, A. & Uchida, N. Whole-brain mapping of direct inputs to midbrain dopamine neurons. *Neuron* **74**, 858-873, doi:10.1016/j.neuron.2012.03.017 (2012).
4 Do, J. P. *et al.* Cell type-specific long-range connections of basal forebrain circuit. *eLife* **5**, doi:10.7554/eLife.13214 (2016).

5 Kim, E. J., Juavinett, A. L., Kyubwa, E. M., Jacobs, M. W. & Callaway, E. M. Three Types of Cortical Layer 5 Neurons That Differ in Brain-wide Connectivity and Function. *Neuron* **88**, 1253-1267, doi:10.1016/j.neuron.2015.11.002 (2015).

6 DeNardo, L. A., Berns, D. S., DeLoach, K. & Luo, L. Connectivity of mouse somatosensory and prefrontal cortex examined with trans-synaptic tracing. *Nature neuroscience* **18**, 1687-1697, doi:10.1038/nn.4131 (2015).

7 Kim, J.-Y., Grunke, S. D., Levites, Y., Golde, T. E. & Jankowsky, J. L. Intracerebroventricular Viral Injection of the Neonatal Mouse Brain for Persistent and Widespread Neuronal Transduction. *Journal of Visualized Experiments : JoVE*, 51863, doi:10.3791/51863 (2014).

8 Wall, N. R., Wickersham, I. R., Cetin, A., De La Parra, M. & Callaway, E. M. Monosynaptic circuit tracing in vivo through Cre-dependent targeting and complementation of modified rabies virus. *Proceedings of the National Academy of Sciences of the United States of America* **107**, 21848-21853, doi:10.1073/pnas.1011756107 (2010).

9 Miyamichi, K. *et al.* Dissecting local circuits: parvalbumin interneurons underlie broad feedback control of olfactory bulb output. *Neuron* **80**, 1232-1245, doi:10.1016/j.neuron.2013.08.027 (2013).

10 Ogawa, Sachie K., Cohen, Jeremiah Y., Hwang, D., Uchida, N. & Watabe-Uchida, M. Organization of Monosynaptic Inputs to the Serotonin and Dopamine Neuromodulatory Systems. *Cell Reports* **8**, 1105-1118, doi:https://doi.org/10.1016/j.celrep.2014.06.042 (2014).

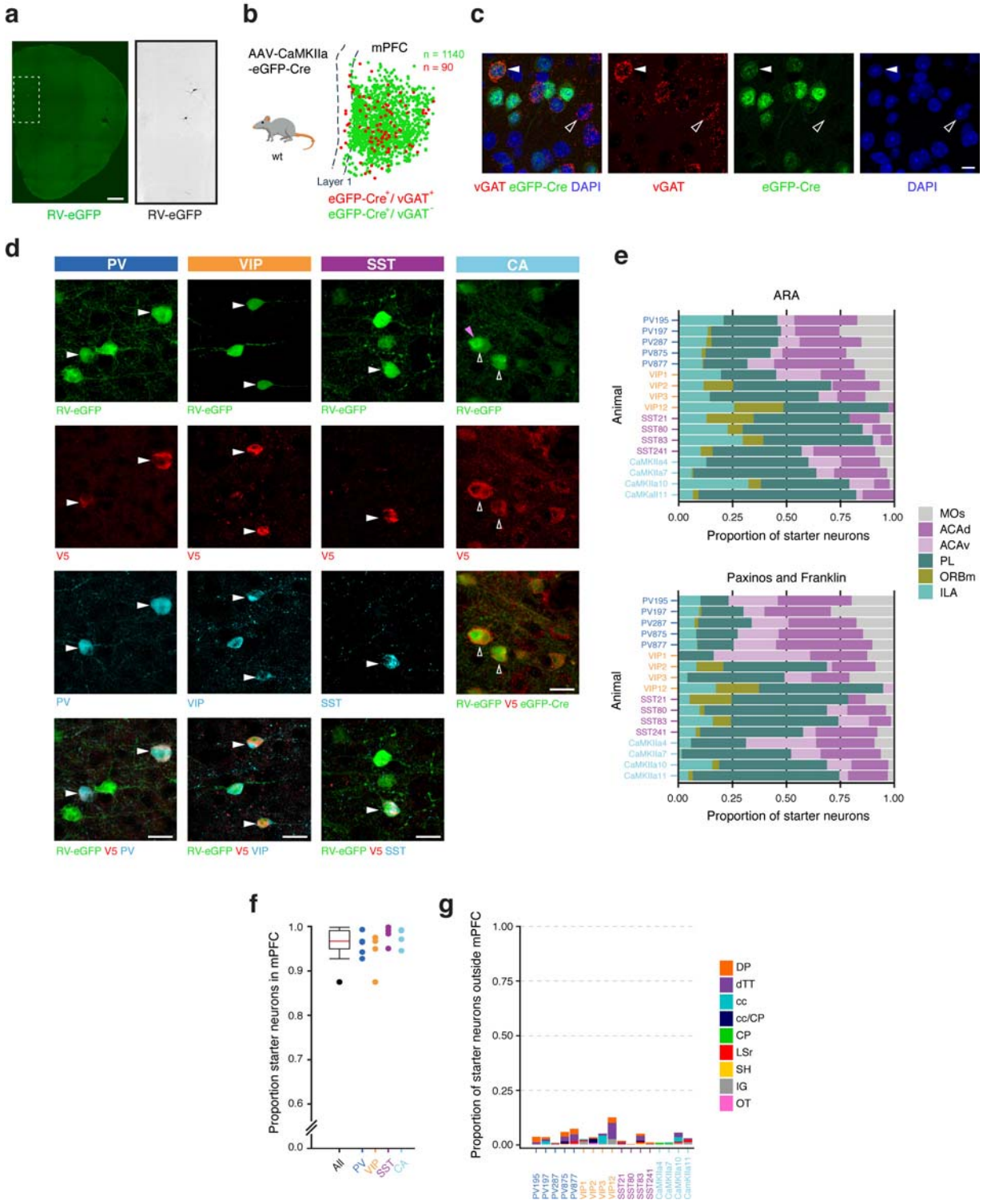

Supplementary Fig. 2

Evaluation of the RV system and mapping of starter neurons

(**a**) Evaluation of the viral batches used in the current study. AAV-DIO-TVA-V5-RG was injected into the mPFC of wt mice (n = 3). Three weeks later RV-eGFP was injected at the same location. No neurons co-expressing V5 and RV-eGFP were detected, but a few neurons expressing only RV-eGFP (4, 19, and 38, respectively) were detected at the injection site. This indicates a lack of expression of TVA in the absence of Cre, and minute RV transduction in the absence of TVA. Right: magnification of outlined area in left.

(**b-c**) Evaluation of the AAV-CaMKIIa-eGFP-Cre. AAV-CaMKIIa-eGFP-Cre was injected into the mPFC of wt mice (n = 2), and RNA-FISH for vGAT was performed. Co-localization of eGFP-Cre and vGAT was detected in a proportion of the neurons (8.30 ± 0.99%; 107 / 1413 neurons, data from 2 mice).
(**b**) Schematic of the localization of detected eGFP-Cre^{+}/vGAT^{-} (green) and eGFP-Cre^{+}/vGAT^{+} (red) neurons, respectively, in the mPFC of one mouse (one 14 µm section).
(**c**) Filled arrowhead: eGFP-Cre^{+}/vGAT^{+} mPFC neuron. Open arrowhead: eGFP-Cre^{-}/vGAT^{+} mPFC neuron.
(**d**) Channel split of images in **Fig. 1f**. Filled arrowheads: starter neurons in the mPFC co-expressing V5 and RV-eGFP and the respective IN marker (PV, SST or VIP). Open arrowheads: excitatory starter neurons in the mPFC co-expressing V5 and RV-eGFP. Pink arrowhead: The fusion protein eGFP-Cre (expressed from the AAV-CaMKIIa-eGFP-Cre) is expressed in the nucleus of excitatory starter neurons. Local input neurons express only RV-eGFP. The V5 is fused to the TVA receptor and therefore detected wherever the receptor is expressed in the neurons (that is, not only at the cell bodies). Images from a representative animal from each group, replicated in PV: n = 5, VIP, SST, CA: = 4 animals / group.
(**e**) Distribution of the starter neurons (expressing V5 and RV-eGFP) within the mPFC subregions in the animals (n = 17) included in the whole-brain mapping of inputs. 1.00 = all detected starter neurons detected within the mPFC. The mapping highlights the differential delineation of the mPFC subregions in the two atlases. In particular, Paxinos and Franklin places fewer neurons in the ILA and more neurons in the ACAv.
(**f**) Boxplot of the proportion starter neurons detected within the mPFC in the animals (n = 17) included in the whole-brain mapping of inputs. Boxplots: center line (white), median; edges, upper and lower quartiles; whiskers, largest and smallest value no further than 1.5× IQR of the edges; dot, outlier (a VIP animal; black dot). The data for the individual animals are also shown. One dot = one animal.
(**g**) Distribution of starter neurons outside the mPFC subregions (n = 17 animals).
Scale bars: 500 µm in (**a**), 50 µm in (**c**), and 20 µm in (**d**).

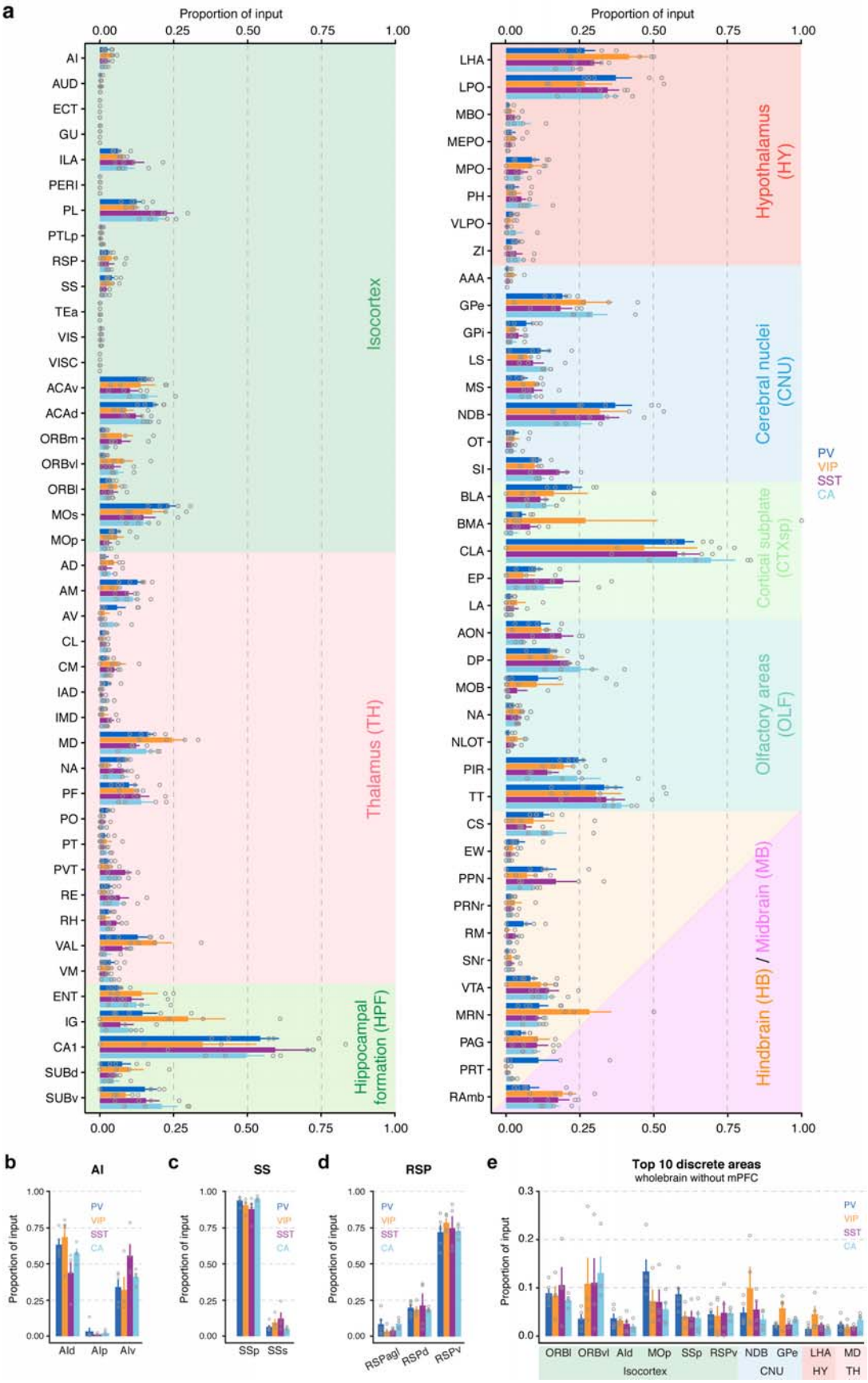
a
Proportion of input
0.00
0.25
0.50
0.75
1.00
AI
AUD
ECT
GU
ILA
PERI
PL
PTLp
RSP
SS
TEa
VIS
VISC
ACAv
ACAd
ORBm
ORBvl
ORBl
MOs
MOp
AD
AM
AV
CL
CM
IAD
IMD
MD
NA
PF
PO
PT
PVT
RE
RH
VAL
VM
ENT
IG
CA1
SUBd
SUBv
Isocortex
Thalamus (TH)
Hippocampal formation (HPF)
LHA
LPO
MBO
MEPO
MPO
PH
VLPO
ZI
AAA
GPe
GPi
LS
MS
NDB
OT
SI
BLA
BMA
CLA
EP
LA
AON
DP
MOB
NA
NLOT
PIR
TT
CS
EW
PPN
PRNr
RM
SNr
VTA
MRN
PAG
PRT
RAmb
Hypothalamus (HY)
Cerebral nuclei (CNU)
Cortical subplate (CTXsp)
Olfactory areas (OLF)
Hindbrain (HB) / Midbrain (MB)
PV
VIP
SST
CA
b
AI
AId
AIp
AIv
c
SS
SSp
SSs
d
RSP
RSPagl
RSPd
RSPv
e
Top 10 discrete areas
wholebrain without mPFC
ORBl
ORBvl
AId
MOp
SSp
RSPv
NDB
GPe
LHA
MD
Isocortex
CNU
HY
TH

Supplementary Fig. 3

Whole-brain mapping of input to the mPFC

(**a**) Whole-brain representation of the proportion of RV-eGFP-labeled input in discrete brain regions. The proportions represent the number of input neurons in a discrete brain region normalized to the total number of input neurons detected in a higher prioritized level (color-coded) in the brain structure hierarchal tree developed in the ARA.
(**b**) The proportion of RV-eGFP input in the divisions of the AI.
(**c**) The proportion of RV-eGFP input in the divisions of the SS.
(**d**) The proportion of RV-eGFP input in the divisions of the RSP.
(**e**) The top 10 discrete input regions. 6/10 regions are cortical regions.
2% cutoff applied for all regions except isocortex in (**a**). Data from PV: n = 5, VIP, SST, CA: n = 4 animals / group in (**a-e**). Data shown as mean ± s.e.m, grey circles denote individual animals in (**a-e**). For abbreviations, see Supplementary Table 4.

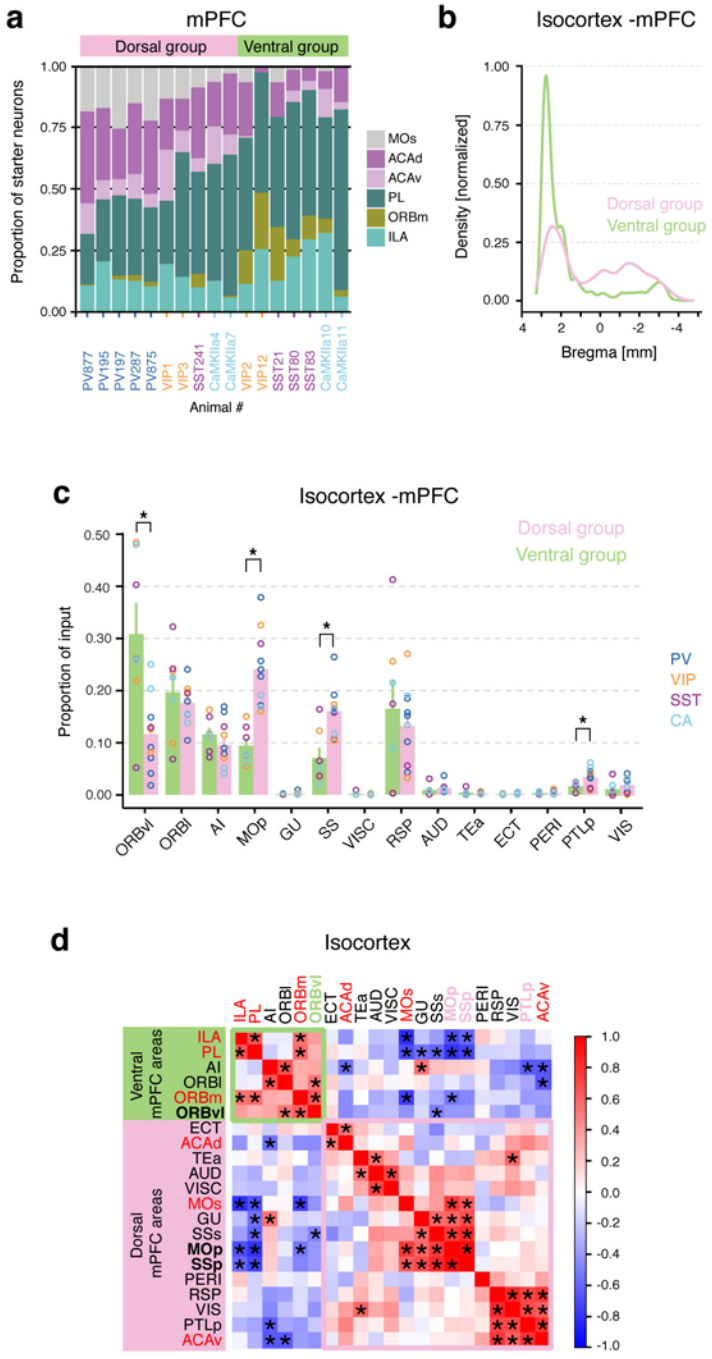

Supplementary Fig. 4

Dorsal–ventral division of the mPFC; differential cortical innervation of the divisions

(**a**) Based on the anatomical distribution of the starter neurons within the mPFC subregions, the animals were divided into a dorsal group (pink; n = 10 animals), and a ventral group (green; n = 7 animals), respectively (see **Methods** for details).
(**b**) The density (normalized) of cortical RV-eGFP labeled input neurons along the A-P axis in the dorsal (pink) and ventral (green) groups (RV-eGFP labeled neurons in the mPFC are excluded). Bin width: 0.16 mm.
(**c**) Detailed analysis of the cortical input pattern for the dorsal (pink), and the ventral (green), animal groups. A two-sided Student's *t*-test was used to generate *P* values. No correction for multiple comparisons was applied. See **Supplementary Table 2** for statistical values.
(**d**) Spearman Correlation matrix and hierarchal clustering (average method) investigating the co-variance of the proportion of input neurons in the regions of the isocortex. Red lettering; mPFC subregions, black lettering; cortical regions, pink lettering; cortical regions with a significantly higher proportion input to the dorsal mPFC, green lettering; cortical regions with

a significantly higher proportion input to the ventral mPFC. Data from 17 animals, sign. level 0.05. Red: positive correlation, blue: negative correlation.
Data from dorsal: n = 10, ventral: n = 7 animals / group in (**b-c**). *P < 0.05, data shown as mean ± s.e.m, circles denote individual animals in (**c**).

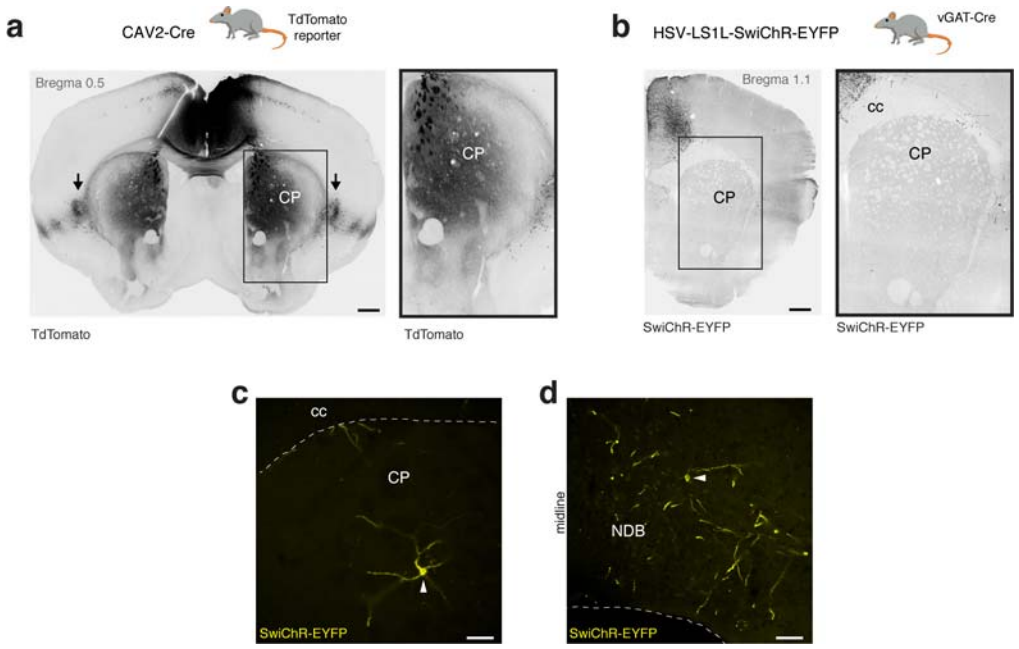

Supplementary Fig. 5

Investigation of monosynaptic projections from STR to mPFC

(**a**) Left: CAV2-Cre was abundantly injected (bilaterally) into the mPFC of TdTomato reporter mice (n = 2). Extensive TdTomato labeling could be detected throughout the brain, including in projections passing through the STR (ACB and CP). However, very few TdTomato labeled cell bodies were detected in the STR (ACB: n = 4 TdTomato+ neurons; CP: n = 7 TdTomato+ neurons). Note the prominent TdTomato labeling in e.g., neurons in the CLA projecting to the mPFC (black arrows). Right: magnification of outlined area in left. Images from a representative animal, replicated in 2 animals.
(**b-d**) HSV-LS1L-SwiChR-EYFP was injected (unilaterally) into the mPFC of vGAT-Cre mice. Images from a representative animal, replicated in 2 animals.
(**b**) Left: HSV-1 labeling could be detected in VGAT-expressing (putative local inhibitory) neurons in the mPFC. Very few labeled neurons could be detected in the STR (ACB: n = 0 labelled neurons, CP: n = 2 labeled neurons in one animal, 1 in the second animal). Right: magnification of outlined area in the left.
(**c**) One of the labeled neurons (white arrowhead) in the STR in the experiment in (**b**). Midline to the left.
(**d**) HSV-1 labeling could be detected in VGAT-expressing long-projecting neurons in subcortical structures. White arrowhead: mPFC projecting VGAT-expressing neuron in the NDB.
Scale bars: 500 µm in (**a**) and (**b**), 50 µm in (**c**) and (**d**).

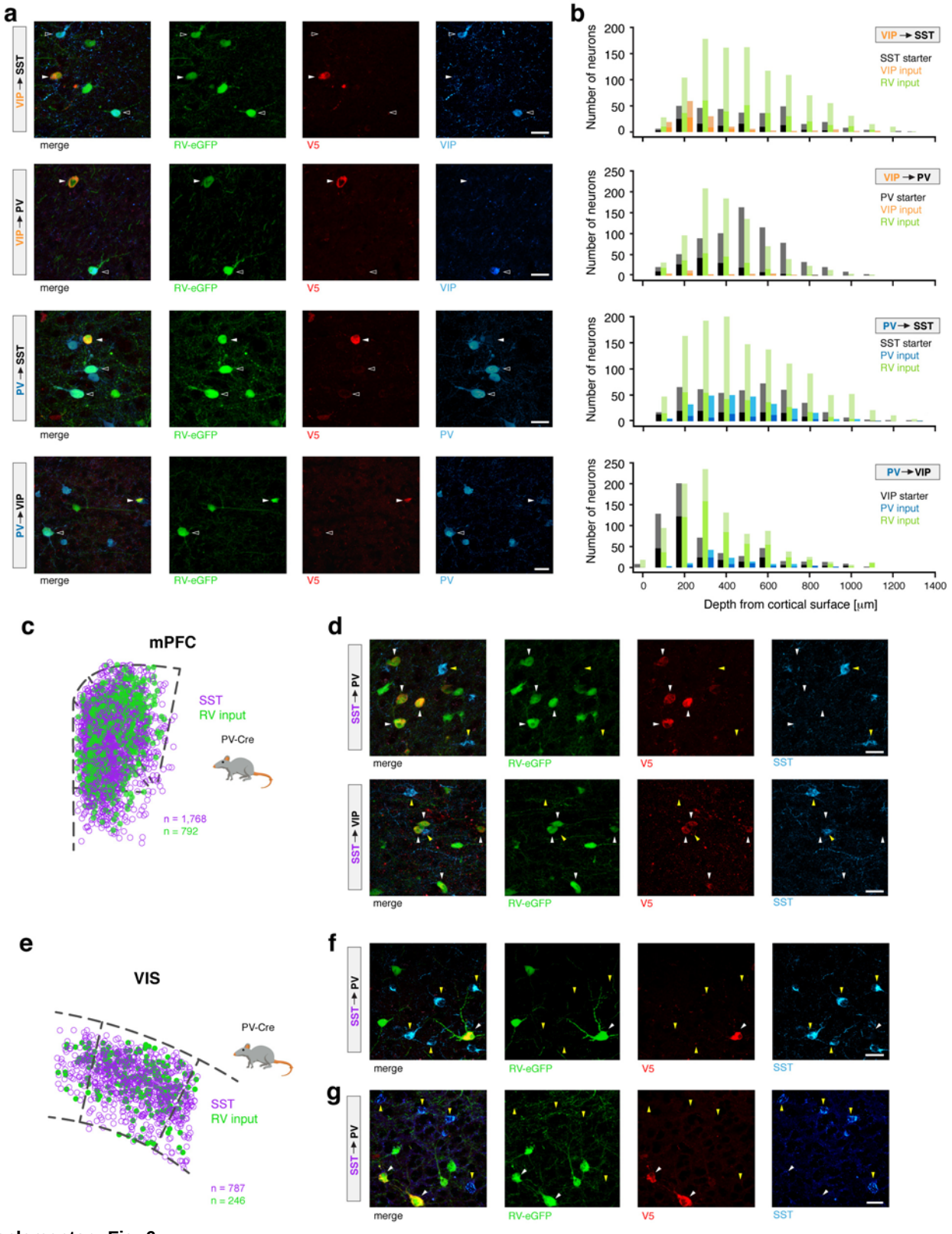

Supplementary Fig. 6

RV tracing of connectivity between IN subtypes in mouse mPFC and VIS

(**a**) Detection of monosynaptic connections between mPFC IN subtypes. Channel split of images in **Fig. 3c**. Filled arrowheads: starter neurons expressing V5 and RV-eGFP; open arrowheads: inhibitory input neurons expressing RV-eGFP

and a specific IN marker. Images from a representative animal from each group, replicated in PV, SST, VIP: n = 2 animals / group, 15-22 sections / animal.
(**b**) Distribution of starter neurons (black), RV-eGFP labeled input neurons (green) and RV-eGFP labeled input neurons of a specific IN subtype (orange or blue) throughout the depth of the mPFC. Absolute cell counts binned per 100 µm from the cortical surface. Data from PV, SST, VIP: n = 2 animals / group. The cell counts for the two animals are stacked in each bar (animal #1: dark colors, animal #2: light colors).
(**c-d**) Immunohistochemical investigation of local SST input to mPFC IN subtypes.
(**c**) Schematic of the localization of detected SST INs (purple), and RV-eGFP labeled local input neurons (green) in a representative PV-Cre mouse (22 superimposed brain sections).
(**d**) Investigation of local SST input to mPFC PV INs (top row: PV-Cre mouse) and to VIP INs (bottom row: VIP-Cre mouse). White arrowheads: starter neurons (expressing V5 and RV-eGFP), yellow arrowheads: SST expressing INs. Images from a representative animal from each group, replicated in PV, VIP: n = 2 animals / group, 15-22 sections / animal. Note the lack of RV-eGFP labelling in the SST INs.
(**e-f**) Immunohistochemical investigation of local SST input to PV INs in the VIS.
Schematic of the localization of detected SST INs (purple), and RV-eGFP labeled local input neurons (green) in a representative PV-Cre mouse (13 superimposed brain sections).
(**f**) White arrowheads: starter neurons (expressing V5 and RV-eGFP), yellow arrowheads: SST expressing INs. Note the lack of RV-eGFP labelling in the SST INs. Images from a representative animal, replicated in 2 animals, 13-14 sections / animal.
(**g**) Investigation of local SST input to PV INs in the VIS using RNA-FISH to detect Sst expression. White arrowheads: starter neurons (expressing V5 and RV-eGFP), yellow arrowheads: Sst expressing INs. Note the lack of RV-eGFP labelling in the Sst-expressing INs. Image from a representative animal, replicated in 2 animals, 4 sections / animal.
Scale bars: 25 µm in (**a**), (**d**), (**f**), and (**g**).

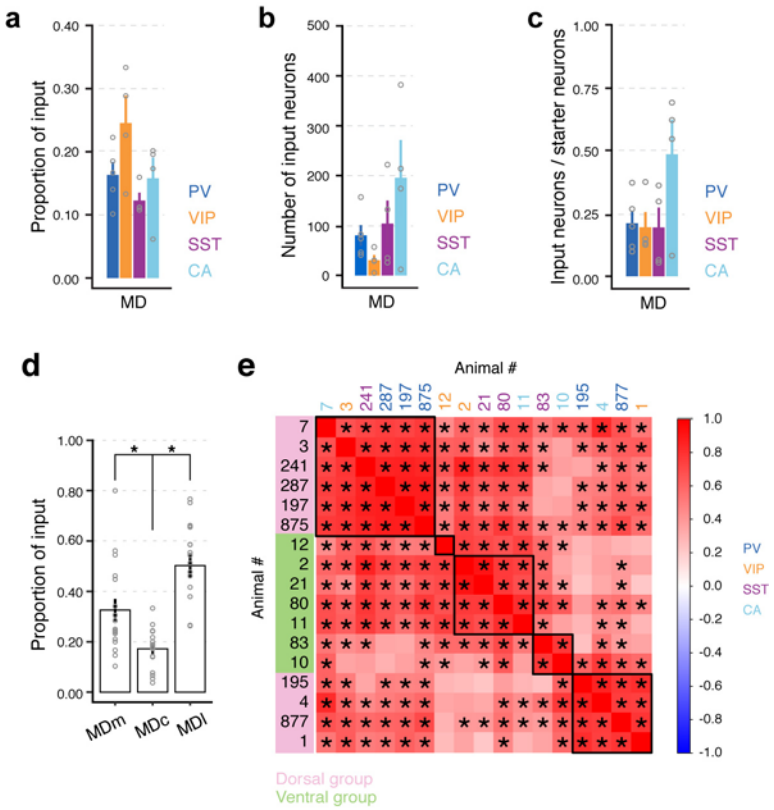

Supplementary Fig. 7

MD targeting of mPFC and dissociation of the thalamic input to dorsal vs. ventral mPFC

(**a-c**) Input from the MD targeting the mPFC investigated in three different ways.
(**a**) Proportion of the thalamic RV-eGFP labeled input being derived from the MD.
(**b**) The number of RV-eGFP labeled input neurons detected in the MD.
(**c**) The relationship between the number of starter neurons detected in the mPFC and RV-eGFP labelled input neurons detected in the MD (input neuron / starter neuron ratio).
(**d**) The distribution of RV-eGFP labeled input neurons within the divisions of the MD, independent of mPFC cell type targeted (n = 17 animals). The MDm and the MDl provide significantly more input than the MDc. A two-sided Student's *t*-test was used to generate *P* values. No correction for multiple comparisons was applied. See **Supplementary Table 2** for statistical values.
(**e**) Spearman Correlation matrix and hierarchal cluster analysis (average method) of the 17 animals based on their thalamic input distribution. No clusters are identified based on animal group, that is, based on the mPFC cell type targeted, but instead there is a high degree of positive correlation between all animals, indicating a high similarity in the animals' thalamic input patterns. (The clusters identified (black outlines) reflect the dorsal (pink) vs. ventral (green) position of the starter neurons in the animals). Sign. level 0.05. Red: positive correlation, blue: negative correlation.
Data from PV: n = 5, VIP, SST, CA: n = 4 animals / group in (**a-c**). **P* < 0.05, data shown as mean ± s.e.m, grey circles denote individual animals in (**a-d**).

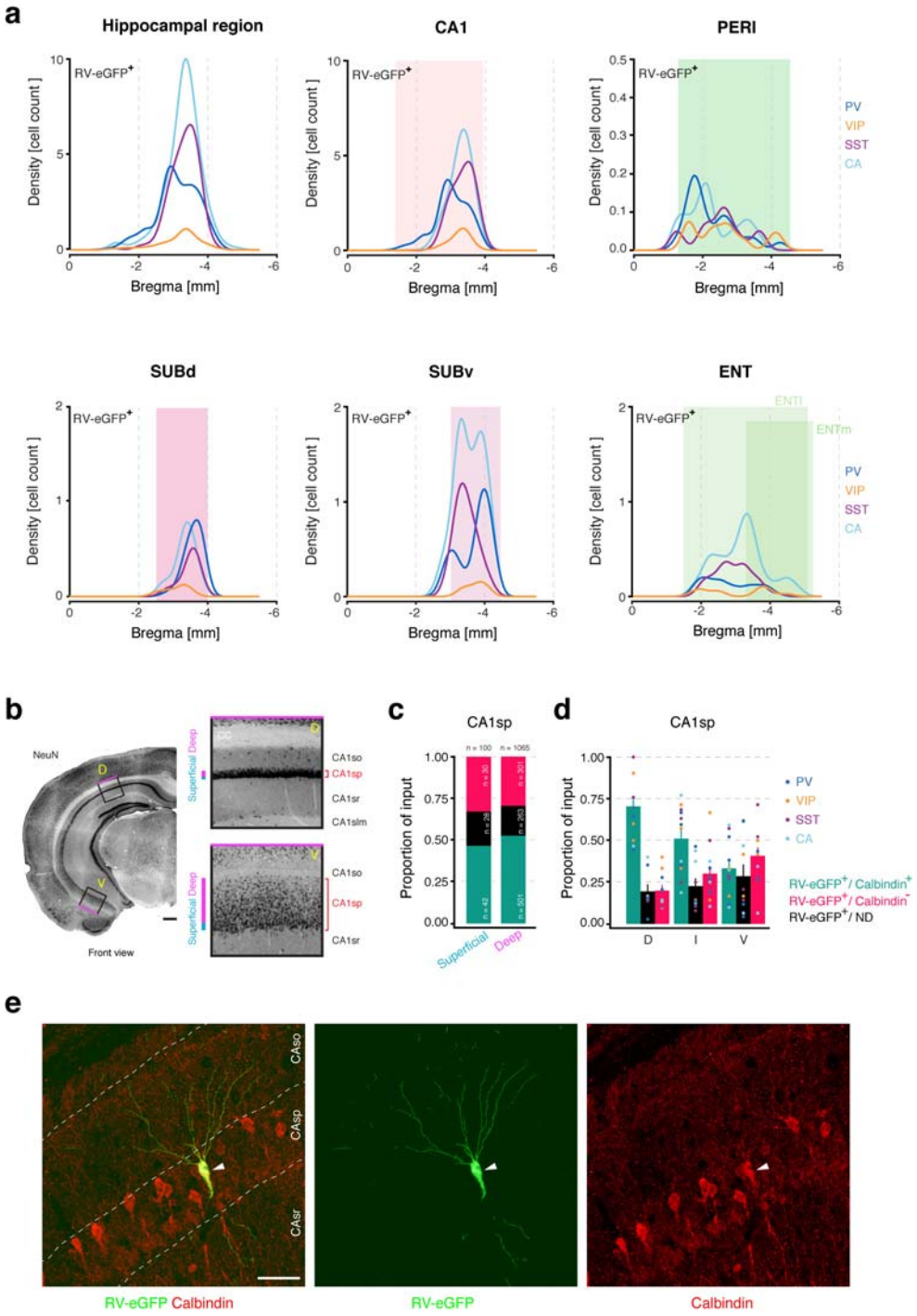

Supplementary Fig. 8

Input from the hippocampal region

(**a**) Cell count density plot (Gaussian kernel) of the RV-eGFP labeled input in the hippocampal region, and in specific discrete regions therein, as detected along the A-P axis (graph for Hippocampal region replicated from **Fig. 6d**). Bin width: 0.05 mm. Shaded areas: A-P extent of the respective region. Data from PV: $n = 5$, VIP, SST, CA: $n = 4$ animals / group.
(**b**) Left; Coronal section immunostained for NeuN for illustration of the dorsal (D) and ventral (V) parts of the CA1. Right; outlined areas in left. The sublayers of the CA1sp (superficial, turquoise; deep, pink) display variation within the CA1. The CA1sr - CA1sp border was used as reference point for the radial division and for anatomical mapping of the RV-eGFP labeled input neurons within, the CA1sp.
(**c**) The expression of calbindin in RV-eGFP labeled input neurons in the superficial and deep sublayers of the CA1sp. 1.00 represents all RV-eGFP labeled neurons in the deep and in the superficial sublayer of the CA1sp, respectively. Data from 12

animals; PV, VIP, SST, CA: *n* = 3 animals / group. Colors as in (**d**).
(**d**) The expression of calbindin in RV-eGFP labeled input neurons in the dorsal (D), intermediate (I) and ventral (V) divisions of the CA1, respectively. 1.00 represents all RV-eGFP neurons in the respective division of the CA1sp. ND; not determined, i.e., ambiguous expression. Data from 12 animals; PV, VIP, SST, CA: *n* = 3 animals / group.
(**e**) A calbindin-expressing RV-eGFP labeled input neuron in the deep subdivision of the CA1sp providing input to mPFC SST INs (SST-Cre mouse). Image from a representative animal, replicated in PV, VIP, SST, CA: n = 3 animals / group, 6-12 sections / animal.
Scale bar: 500μm in (**b**), 50 μm in (**e**). Data shown is mean ± s.e.m, circles denote individual animals in (**d**).

Supplementary Table 2. Statistical values

Figure	Area	t-value	Degrees of freedom	P-value	n
Fig.S3 b)	**MOp**	t = 5.4675	df = 13.866	p-value = 8.581e-05	Ventral group n=10 animals, Dorsal group n=7 animals.
	ORBvl	t = -3.0248	df = 7.7629	p-value = 0.01703	
	SS	t = 3.5906	df = 12.004	p-value = 0.003708	
	AI	t = -1.0663	df = 14.974	p-value = 0.3032	
	PTLp	t = 2.5183	df = 13.98	p-value = 0.0246	
	RSP	t = -0.54349	df = 8.2087	p-value = 0.6012	
	VIS	t = 1.0735	df = 13.747	p-value = 0.3015	
	TEa	t = -0.66468	df = 5.7721	p-value = 0.5319	
	AUD	t = 0.57576	df = 9.358	p-value = 0.5784	
	GU	t = 0.68549	df = 11.745	p-value = 0.5063	
	ECT	t = 2.3039	df = 9.9992	p-value = 0.04397	
	VISC	t = -0.77895	df = 3.0876	p-value = 0.4913	
	PERI	t = -0.016139	df = 14.449	p-value = 0.9873	
Fig.4 e)	**VIP.CA**	t = 2.0593	df = 3.4446	p-value = 0.1198	n= 17 animals, (PV: 4, VIP: 3, SST: 3, CA: 3).
	VIP.PV	t = 3.1388	df = 4.9865	p-value = 0.0258	
	VIP.SST	t = 3.621	df = 3.9683	p-value = 0.02264	
Fig.5 d)	**MDl**	t = 3.0091	df = 7.7118	p-value = 0.01757	Ventral group n=10 animals, Dorsal group n=7 animals.
	MDm	t = -2.9995	df = 7.1222	p-value = 0.01955	
	MDc	t = -0.53252	df = 13.823	p-value = 0.6028	
Fig.S6 d)	**MDm.MDc**	t = 3.1953	df = 21.984	p-value = 0.00418	n= 17 animals
	MDl.MDc	t = 8.484	df = 22.441	p-value = 1.876e-08	

Supplementary Table 3. Antibody list

Primary Antibodies

Host	Target	Company	Catalogue #	Lot #	Dilution	Manufacture Validation
Rabbit	Parvalbumin	Swant	PV27 (previously 25)	5.10	1:1000	https://www.swant.com/pdfs/PV27_Rabbit_anti_Parvalbumin.pdf
Guinea Pig	Parvalbumin	Synaptic systems	195 004	-	1:1000	https://www.sysy.com/products/parvalbumin/facts-195004.php
Rat	Somatostatin	Millipore	MAB354	2326265	1:500	http://www.merckmillipore.com/SE/en/product/Anti-Somatostatin-Antibody-clone-YC7,MM_NF-MAB354
Goat	Choline Acetyltransferase	Millipore	AB144P	2280814, 2558394	1:300	http://www.merckmillipore.com/SE/en/product/Anti-Choline-Acetyltransferase-Antibody,MM_NF-AB144P
Rabbit	FoxP2	Abcam	ab16046	GR91556-1	1:1000	https://www.abcam.com/foxp2-antibody-ab16046.html
Rabbit	Calretinin	Swant	7697 (previously 7699)	18299	1:1000	https://www.swant.com/pdfs/Rabbit_anti_calretinin_7697.pdf
Goat	V5	Bethyl Lab.	A190-119A	A190-119A-4	1:1000	https://www.bethyl.com/product/A190-119A
Goat	Somatostatin	Santa Cruz	sc-7819	B0413	1:250	https://www.scbt.com/scbt/product/somatostatin-antibody-d-20?bvstate=pg:2/ct:r
Chicken	V5	Abcam	ab9113	GR203305-4	1:500	https://www.abcam.com/v5-tag-antibody-ab9113.html
Rabbit	VIP	Immunostar	20077	1513001	1:200	http://www.immunostar.com/shop/content/pdf/20077-1744002.pdf
Guinea Pig	Parvalbumin	Swant	GP 72	-	1:1000	https://www.swant.com/pdfs/GP72_Guinea_pig_anti_parvalbumin.pdf
Rabbit	GFP	Invitrogen	A6455	1900253	1:1000	https://www.thermofisher.com/antibody/product/GFP-Antibody-Polyclonal/A-6455
Rabbit	Calbindin- 28K	Millipore	AB1778	2390391	1:500	http://www.merckmillipore.com/SE/en/product/Anti-Calbindin-D-28K-Antibody,MM_NF-AB1778
Mouse	NeuN	Millipore	AB377	2279235	1:500	http://www.merckmillipore.com/SE/en/product/Anti-NeuN-Antibody-clone-A60,MM_NF-MAB377

Secondary Antibodies

Host	Target	Fluorophore	Company	Code #	Dilution
Donkey	Rabbit	Cy3	Jackson	711-165-152	1:1000
Donkey	Rabbit	Cy5	Jackson	711-175-152	1:1000
Donkey	Rabbit	DyLight 405	Jackson	711-475-152	1:500
Donkey	Rabbit	DyLight 488	Jackson	711-545-152	1:1000
Donkey	Guinea Pig	Cy3	Jackson	706-165-148	1:1000
Donkey	Guinea Pig	Cy5	Jackson	706-175-148	1:1000
Donkey	Guinea Pig	DyLight 405	Jackson	706-475-148	1:500
Donkey	Rat	Cy3	Jackson	712-165-153	1:1000
Donkey	Rat	Cy5	Jackson	712-175-153	1:1000
Donkey	Goat	Cy3	Jackson	705-165-147	1:1000
Donkey	Goat	Cy5	Jackson	705-175-147	1:1000
Donkey	Goat	Alexa Fluor 405	Jackson	705-475-147	1:500
Donkey	Chicken	Cy3	Jackson	703-165-155	1:1000
Donkey	Chicken	Cy5	Jackson	703-175-155	1.1000
Donkey	Mouse	Cy3	Jackson	715-165-151	1.1000
Donkey	Mouse	Cy5	Jackson	715-175-151	1.1000

Supplementary Table 4. ARA Nomenclature

ISO	**Isocortex**
MOp	Primary motor area
MOs	Secondary motor area
SS	Somatosensory areas
SSp	Primary somatosensory area
SSs	Supplemental somatosensory area
ILA	Infralimbic area
GU	Gustatory areas
VISC	Visceral area
AUD	Auditory areas
VIS	Visual areas
ACA	Anterior cingulate area
ACAd	Anterior cingulate area, dorsal part
ACAv	Anterior cingulate area, ventral part
PL	Prelimbic area
ORB	Orbital area
ORBl	Orbital area, lateral part
ORBm	Orbital area, medial part
ORBv	Orbital area, ventral part
ORBvl	Orbital area, ventrolateral part
AI	Agranular insular area
AId	Agranular insular area, dorsal part
AIp	Agranular insular area, posterior part
AIv	Agranular insular area, ventral part
RSP	Retrosplenial area
RSPd	Retrosplenial area, dorsal part
RSPv	Retrosplenial area, ventral part
RSPagl	Retrosplenial area, lateral agranular part
PTLp	Posterior parietal association areas
TEa	Temporal association areas
PERI	Perirhinal area
ECT	Ectorhinal area
OLF	**Olfactory areas**
AOB	Accessory olfactory bulb
AON	Anterior olfactory nucleus
TT	Taenia tecta
TTd	Taenia tecta, dorsal part
TTv	Taenia tecta, ventral part
DP	Dorsal peduncular area
PIR	Piriform area
NLOT	Nucleus of the lateral olfactory tract
COA	Cortical amygdalar area
PAA	Piriform-amygdalar area
TR	Postpiriform transition area
MOB	Main olfactory bulb
HPF	**Hippocampal formation**
HIP	Hippocampal region
CA	Ammon's Horn
CA1	Field CA1
CA1slm	Field CA1, stratum lacunosum-moleculare
CA1so	Field CA1, stratum oriens
CA1sp	Field CA1, pyramidal layer
CA1sr	Field CA1, stratum radiatum
CA2	Field CA2
CA3	Field CA3
DG	Dentate gyrus

FC	Fasciola cinerea
IG	Induseum griseum
RHP	**Retrohippocampal region**
ENT	Entorhinal area
ENTl	Entorhinal area, lateral part
ENTm	Entorhinal area, medial part, dorsal zone
ENTmv	Entorhinal area, medial part, ventral zone
PAR	Parasubiculum
POST	Postsubiculum
PRE	Presubiculum
SUB	Subiculum
SUBd	Subiculum, dorsal part
SUBv	Subiculum, ventral part
CTXsp	**Cortical Subplate**
CLA	Claustrum
EP	Endopiriform nucleus
EPd	Endopiriform nucleus, Dorsal part
EPv	Endopiriform nucleus, Ventral part
LA	Lateral amygdalar nucleus
BLA	Basolateral amygdalar nucleus
BMA	Basomedial amygdalar nucleus
PA	Posterior amygdalar nucleus
CNU	**Cerebral nuclei**
STR	**Striatum**
CP	Caudoputamen
ACB	Nucleus accumbens
OT	Olfactory tubercle
LS	Lateral septal nucleus
LSr	Lateral septal nucleus, rostral
SH	Septohippocampal nucelus
sAMY	**Striatum like amygdalar nuclei**
AAA	Anterior amygdalar area
BA	Bed nucleus of the accessory olfactory tract
CEA	Central amygdalar nucleus
IA	Intercalated amygdalar nucleus
MEA	Medial amygdalar nucleus
PAL	**Pallidum**
GP	Globus Pallidus
GPe	Globus Pallidus, External segment
GPi	Globus Pallidus, Internal segment
SI	Substantia innominata
MA	Magnocellular nucleus
MS	Medial septal nucleus
NDB	Diagonal band nucleus
BST	Bed nuclei of the stria terminalis
TH	**Thalamus**
DORsm	*Thalamus, Sensory-Motor cortex related*
VENT	*Ventral group of dorsal thalamus*
VAL	Ventral anterior-lateral complex of the thalamus
VM	Ventral medial nucleus of the thalamus
VP	Ventral posterior complex of the thalamus
SPF	Subparafascicular nucleus
SPA	Subparafascicular area
PP	Peripeduncular nucleus
DORpm	*Thalamus, Polymodal association cortex related*
LAT	*Lateral group of the dorsal thalamus*
LP	Lateral posterior nucleus of the thalamus
PO	Posterior complex of the thalamus

POL	Posterior limiting nucleus of the thalamus
SGN	Suprageniculate nucleus
ATN	*Anterior group of the dorsal thalamus*
AV	Anteroventral nucleus of the thalamus
AM	Anteromedial nucleus of the thalamus
AD	Anterodorsal nucleus of the thalamus
IAM	Interanteromedial nucleus of the thalamus
IAD	Interanterodorsal nucleus of the thalamus
LD	Lateral dorsal nucleus of the thalamus
MED	Medial group of the dorsal thalamus
IMD	Intermediodorsal nucleus of the thalamus
MD	Mediodorsal nucleus of the thalamus
MDc	Mediodorsal nucleus of the thalamus, central part
MDl	Mediodorsal nucleus of the thalamus, lateral part
MDm	Mediodorsal nucleus of the thalamus, medial part
SMT	Submedial nucleus of the thalamus
PR	Perireuniens nucleus
MTN	*Midline group of the dorsal thalamus*
PVT	Paraventricular thalamic nucleus
PT	Paratenial nucleus
RE	Nucleus of reunions
ILM	*Intralaminar group of the dorsal thalamus*
RH	Rhomboid nucleus
CM	Central medial nucleus of the thalamus
PCN	Paracentral nucleus of the thalamus
CL	Central lateral nucleus of the thalamus
PF	Parafascicular nucleus
RT	Reticular nucleus of the thalamus
HY	**Hypothalamus**
MEPO	Median preoptic nucleus
MPO	Medial preoptic area
VLPO	Ventrolateral preoptic nucleus
MBO	Mammillary body
PH	Posterior hypothalamic nucleus
LHA	Lateral hypothalamic area
LPO	Lateral preoptic area
ZI	Zona incerta
MB	**Midbrain**
SNr	Substantia nigra, reticular part
VTA	Ventral tegmental area
MRN	Midbrain reticular nucleus
PAG	Periaqueductal gray
PRT	Pretectal region
EW	Edinger-Westphal nucleus
PPN	Pedunculopontine nucleus
RAmb	Midbrain raphé nuclei
HB	**Hindbrain**
CS	Superior central nucleus raphé
PRNr	Pontine reticular nucleus
RM	Nucleus raphé magnus
pf	fasciculus retroflexus
cc	corpus callosum